

Lab on a Chip

Accepted Manuscript

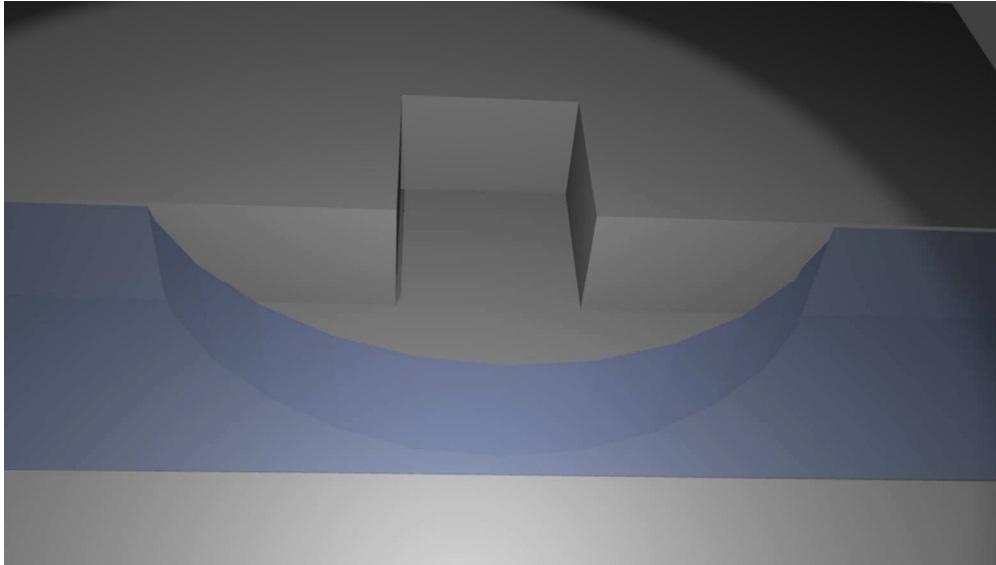


This is an *Accepted Manuscript*, which has been through the Royal Society of Chemistry peer review process and has been accepted for publication.

Accepted Manuscripts are published online shortly after acceptance, before technical editing, formatting and proof reading. Using this free service, authors can make their results available to the community, in citable form, before we publish the edited article. We will replace this *Accepted Manuscript* with the edited and formatted *Advance Article* as soon as it is available.

You can find more information about *Accepted Manuscripts* in the [Information for Authors](#).

Please note that technical editing may introduce minor changes to the text and/or graphics, which may alter content. The journal's standard [Terms & Conditions](#) and the [Ethical guidelines](#) still apply. In no event shall the Royal Society of Chemistry be held responsible for any errors or omissions in this *Accepted Manuscript* or any consequences arising from the use of any information it contains.



A bubble in an advanced growth state inside a microchannel (gray colors) filled with water (bluish colors).

Growth control of sessile microbubbles in PDMS devices

Andreas Volk,^a Massimiliano Rossi,^{*a} Christian J. Kähler,^a Sascha Hilgenfeldt,^b and Alvaro Marin^{*a}

Received Xth XXXXXXXXXXXX 20XX, Accepted Xth XXXXXXXXXXXX 20XX

First published on the web Xth XXXXXXXXXXXX 20XX

DOI: 10.1039/b000000x

In a microfluidic environment, the presence of bubbles is often detrimental to the functionality of the device, leading to clogging or cavitation, but microbubbles can also be an indispensable asset in other applications such as microstreaming. In either case, it is crucial to understand and control the growth or shrinkage of these bodies of air, in particular in common soft-lithography devices based on polydimethylsiloxane (PDMS), which is highly permeable to gases. In this work, we study the gas transport into and out of a bubble positioned in a microfluidic device, taking into account the direct gas exchange through PDMS as well as the transport of gas through the liquid in the device. Hydrostatic pressure regulation allows for the quantitative control of growth, shrinkage, or the attainment of a stable equilibrium bubble size. We find that the vapor pressure of the liquid plays an important role for the balance of gas transport, accounting for variability in experimental conditions and suggesting additional means of bubble size control in applications.

1 Introduction

Bubbles are ubiquitous in our everyday life,¹ in arts,² in engineering,³ and also in microfluidics. Uncontrolled growing bubbles in small devices can fatally disrupt many processes in microfluidics: for example, Shin et al.⁴ performed Polymerase Chain Reactions (PCR) in a microfluidic device and found that the main reason for failure was the formation and growth of bubbles, which they managed to control by coating the surface of their device with substances of low permeability to avoid bubble formation.⁵ However, in other systems such as carbonated drinks or beer, growing bubbles are desired and understanding their formation and growth is crucial to optimize foam formation, taste and texture.^{1,6,7} In other applications, the presence of bubbles is necessary, but their growth (or dissolution) must be under control. That is crucial in micro fuel cells, in which CO₂ bubbles are usually generated and need to be dissolved in the surrounding water solution; the presence of other gas species in the liquid can be detrimental to this process, stabilizing the bubbles and preventing their total dissolution.^{8,9}

Other applications require bubbles of specific size at known positions. This is the case in acoustic streaming driven by oscillating microbubbles:^{10–12} A sessile bubble is stabilized in a blind channel or micro-pit and actuated through a piezo transducer to induce bubble oscillations that generate a steady streaming flow in the liquid. Control of the bubble size and

shape is important in order to retain constant flow conditions and a constant bubble response to the chosen driving frequency. On silicon substrates, the bubble is controlled by simply oversaturating the liquid solution.^{13,14} The bubble then grows due to oversaturation until the pressure differences are equilibrated by surface tension, as mandated by Young-Laplace equation. If the system is closed and there are no changes in pressure, concentration or temperature, the bubble should remain stable at a constant radius. Unfortunately that is not the case when working in systems based on polydimethylsiloxane (PDMS): PDMS is by far the most commonly used material for microfluidic applications due to its biocompatibility, ease of fabrication and low price.¹⁵ But it is also a porous medium permeable to gas (and to some degree to liquid).¹⁶ The porosity of PDMS has been used as an advantage for promoting fluid motion due to the evaporation through the pore network¹⁷ or to supply oxygen to cells in PDMS-based bioreactors.¹⁸ However, controlling the growth of bubbles becomes a more complex task. To our knowledge, no strategies have been proposed explicitly in the literature for the control of bubbles in PDMS-based microfluidic devices.

In this paper, we study the stability of sessile microbubbles trapped in blind channels of PDMS devices under different conditions and propose methods based on the control of the hydrostatic pressure inside the device which are easy to implement in any system. Our conclusions are particularly useful for microfluidic applications, which require control of the gas transfer both through a gas-liquid interface as well as a gas-solid interface.

^a Institute for Fluid Mechanics and Aerodynamics, Bundeswehr University Munich, 85577 Neubiberg, Germany, E-mail: a.marin@unibw.de

^b Department of Mechanical Science and Engineering, University of Illinois at Urbana-Champaign, Urbana-Champaign, USA

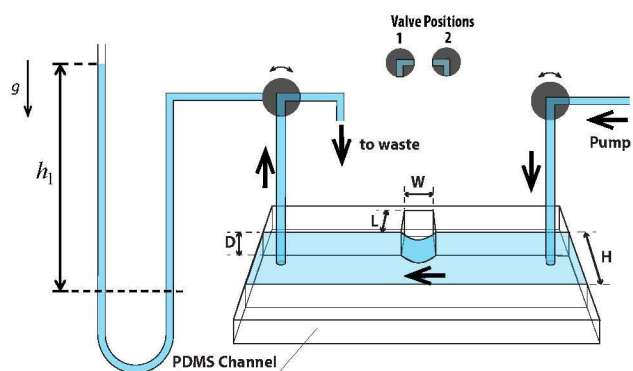


Fig. 1 Experiments are performed on a PDMS channel filled by a syringe pump (or by a pressurized system). With the two-way valves in the position **1**, the PDMS-microchannel is filled with liquid from the pump. As the liquid enters the channel, an air pocket is trapped in the blind side channel forming a sessile bubble. By switching the valves to position **2**, the channel is open to the atmosphere through the open tube at the left side of the sketch. The liquid's pressure is adjusted by moving the flexible tube's end to the desired relative liquid level h_1 .

2 Experimental Setup

Experiments are performed on a PDMS microchannel with a blind side channel and a tubing system to control the filling and liquid pressure, as sketched in Fig. 1. The PDMS device is fabricated using standard soft lithography, as described by Wang *et al.*¹⁹ The main channel has a rectangular cross-section with a depth $D = 100 \mu\text{m}$ and a height $H = 250 \mu\text{m}$. The blind side channel, perpendicular to the main channel and sharing the depth D , has a width $W = 50 \mu\text{m}$ and a height $L = 150 \mu\text{m}$. Both main and blind side channel are completely embedded in PDMS. A PDMS layer of $\sim 4 \text{ mm}$ is separating the channel structure from the surrounding atmosphere. With the only exception of a 2 mm thick PDMS layer which separates the channel from the glass side to which the PDMS-device is attached to. The setup includes two two-way valves and a manometer-style water column to adjust the relative water level h_1 and thus the hydrostatic pressure in the system. With the valves in position **1**, the microchannel is filled with liquid from the pump, remaining unconnected to the water column. Once the channel is filled, an air pocket remains trapped in the side channel forming a quasi-hemicylindrical bubble. In order to study the bubble growth without a net flow across the channel, the valves are then switched to position **2**, which closes the inlet and connects the outlet to the water column. The liquid's pressure is then adjusted by the relative liquid level h_1 . In our experiments this was done by connecting a flexible tube to the outlet valve (tube connected to left valve in Fig. 1). The tube was filled with water up to the open end. Us-

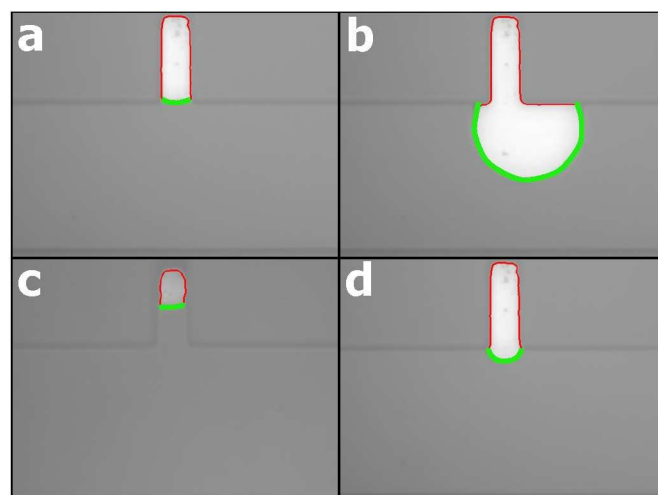


Fig. 2 Bubble volume is calculated by fitting a circle to the gas-liquid interface (green line) and to the gas-solid interface (red line). Each experiment starts at $t = 0$ with the bubble's volume roughly matching the pit's (a). By adjusting the liquid's hydrostatic pressure we can obtain growing (b), shrinking (c), or steady bubbles (d).

ing a vertical positioning system with millimetric resolution, the end of the tube was moved up or down in order to set the relative liquid level to the desired value.

3 Results

Assuming stationary or quasi-stationary conditions, the gas pressure inside the microbubble p_{bub} can be calculated using the Young-Laplace equation:

$$p_{\text{bub}} = p_0 + \rho_1 g h_1 + K \gamma_1 \quad (1)$$

where p_0 is the atmospheric pressure, g is the gravitational acceleration, ρ_1 is the liquid density, γ_1 is the liquid's surface tension and K is the bubble curvature. Since the equilibrium contact angle of water and glycerol in PDMS is close to 90° ,²⁰ we can assume that the bubble is practically cylindrical and therefore $K = 1/a$, where a is the bubble projected radius. From now on we will refer to the last term of Eq. (1) as $p_{\text{YL}} = \gamma_1/a$ or as Young-Laplace pressure. Considering the hydrostatic pressure $p_{\text{hyd}} = \rho_1 g h_1$ the difference between bubble pressure and atmospheric pressure is given by $\Delta p = p_{\text{hyd}} + p_{\text{YL}}$. Each experiment was performed at constant hydrostatic pressure (constant h_1) and started from a microbubble with an almost flat liquid-gas interface (see Fig. 2a). By manipulating the control variables, the bubble can be made to grow (Fig. 2b), shrink (Fig. 2c) or reach a steady state in which the bubble interface adopts an intermediate shape between flat and hemicylindrical (Fig. 2d).

A microscope (Zeiss Axio Imager Z2) and a camera (Zeiss AxioCam HRm) are used to visualize the sessile bubble during the experiments. Each experiment ran for a maximum of 400 seconds, acquiring images at 0.2 fps. For each image, the boundaries of the bubble were extracted with an image processing software and used to determine the bubble volume V_{bub} , the bubble radius a , the liquid-gas area A_1 , and the PDMS-gas area A_s as a function of time. The depth dimension was always assumed to be the nominal depth D of the channel. The bubble radius a was measured performing a circle fit²¹ to the liquid-gas interface (green lines in Fig. 2). Three different liquids have been used: glycerol, air-saturated water, and degassed water. The liquids are chosen to analyze the effects of air solubility and vapor pressure. We used triply deionized water (Milli-Q millipore) for the experiments. Air-saturated water was typically stored in a fridge overnight at circa 10°C. Water was degassed at 0.07 bar for 30 min with a magnetic stirrer; the sample was then immediately inserted in the PDMS device.

3.1 Experiments using Glycerol

The first set of experiments was performed using glycerol as working fluid. Figure 3a shows the bubble volume V_{bub} as a function of time, for different hydrostatic pressures (or relative liquid levels h_1). The values of V_{bub} are normalized to the volume of the blind side channel (or pit) $V_{\text{pit}} = \text{DWL}$, so

that $V_{\text{bub}}/V_{\text{pit}} = 1$ at the beginning of each experiment. Bubbles grow for liquid pressures much lower than atmospheric (negative values of h_1). As we increase the hydrostatic pressure the growth decreases until stable bubbles are achieved. In our experiments we found a range of hydrostatic pressures at which the bubble remains stable within our observation time-scale, spanning from -3710 Pa to -1240 Pa (corresponding to $h_1 = -30$ cm to $h_1 = -10$ cm using the glycerol density of $\rho_1 = 1261$ kg/m³).

From the curves shown in Fig. 3a, we quantify representative bubble growth rates Q_{tot} for different hydrostatic pressures. For growing bubbles, the growth rate of each data set is computed at $V_{\text{bub}}/V_{\text{pit}} = 3$, averaging over the growth in a time interval of 20 s; this is a convenient definition, and the results do not vary significantly when the time interval of the average ensemble is changed. For stable bubbles, the growth rate is zero by definition. For shrinking bubbles, it is quantified at the point where their volume shrinks to 70% of V_{pit} . The respective locations for evaluating Q_{tot} are indicated as black circles in Fig. 3a; the values are plotted against p_{hyd} in Fig. 3b.

Bubble stability manifests in Fig. 3b as a plateau where $Q_{\text{tot}} \approx 0$. In this region, the bubble's curvature decreases as the hydrostatic pressure is increased, so that the bubble's air pressure remains constant and $\Delta p^{\text{air}} \approx 0$. Stable bubbles have an hemicylindrical cross section at the smallest p_{hyd} and an al-

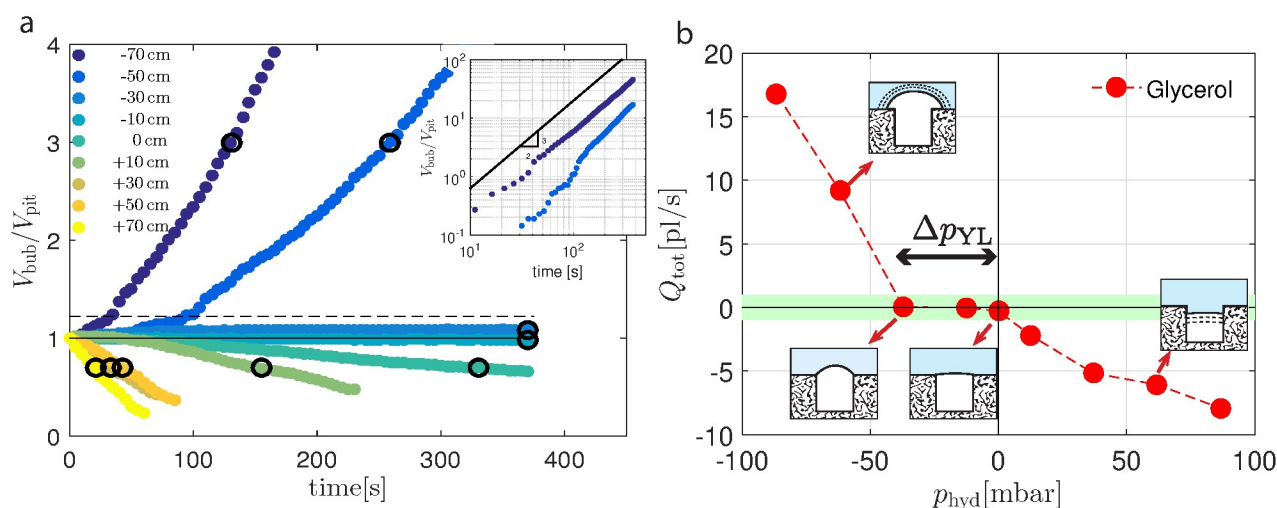


Fig. 3 a) Normalized bubble volume as a function of time for different liquid pressures in the experiments with glycerol. The liquid in the microchannel is connected to a movable liquid column at different heights to obtain different hydrostatic pressures. The black dashed line corresponds to the volume of a semi-cylindrical bubble with $a = W/2$. The black circles correspond to those points where the slope is taken to define the growth rate Q_{tot} . In the insert a log-log graph shows the $V \sim t^{3/2}$ scaling that growing bubbles follow at large time scales. b) Bubble growth rate Q_{tot} as a function of the hydrostatic pressure p_{hyd} in the liquid. The bubble is growing in the upper part ($Q_{\text{tot}} > 0$) and shrinking in the lower half of the plot ($Q_{\text{tot}} < 0$). Bubble stability is achieved for the data points within the green area, where $-\Delta p_{\text{YL}} < p_{\text{hyd}} < 0$; $\Delta p_{\text{YL}} = p_{\text{YL}}(a = W/2) - p_{\text{YL}}(a = \infty)$ and the growth or shrinkage is negligible within the experimental time scale.

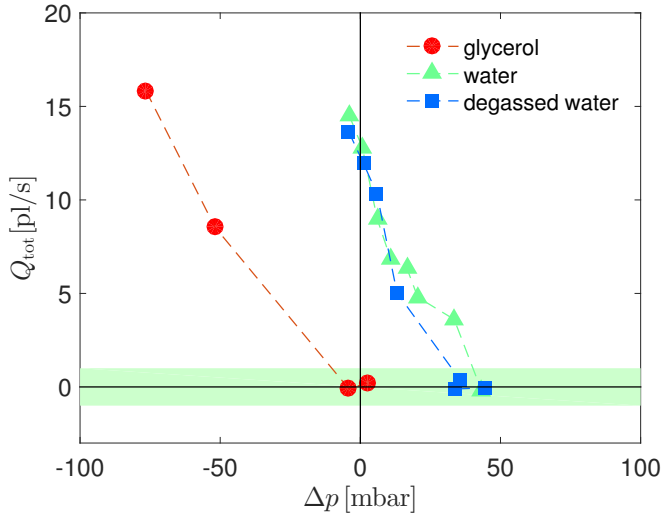


Fig. 4 Bubble growth rate Q_{tot} for glycerol, air-saturated water and degassed water as a function Δp .

most flat shape at $p_{\text{hyd}} = 0$. Therefore, the plateau's width is well approximated by the value of the Young-Laplace pressure of a $a = W/2$ semi-cylindrical bubble, $2\gamma_1/W = 2520$ Pa. Note that at $p_{\text{hyd}} = 0$ ($h_1 = 0$) the bubble shrinks slowly since the bubble is not completely flat and the air partial pressure difference Δp^{air} is positive and equal to the Young-Laplace pressure. Beyond this point, both hydrostatic and Young-Laplace pressure have the same sign and they contribute to increase the bubble's air pressure. Air is then forced through the system and the bubble shrinks into the pit ($Q_{\text{tot}} < 0$), eventually vanishing completely after sufficient time.

3.2 Experiments using Water

Since most applications use aqueous solutions, two more sets of experiments were performed using air-saturated and degassed water as working liquids. In this case, neither gas diffusion nor evaporation can be neglected. Since the diffusivity of vapor in air is three decades larger than that of air in water ($D_{\text{air}}^{\text{w}} = 2 \cdot 10^{-9} \text{ m}^2/\text{s}$ and $D_{\text{vapor}}^{\text{air}} = 0.282 \cdot 10^{-4} \text{ m}^2/\text{s}$), we can safely assume that evaporation is much faster than air diffusion and the bubble is always saturated with vapor. This is indeed the most important difference from the case of glycerol, given that the vapor pressure of glycerol under atmospheric conditions is negligible for our experiments. Therefore, in experiments with volatile liquids, the bubble pressure depends also on the liquid's vapor pressure.

The results are plotted in Fig. 4 as a function of $\Delta p = p_{\text{hyd}} + p_{\text{YL}}$ for $Q_{\text{tot}} > 0$ only. Note that Δp is constant for stable bubbles (see Eq. (1)) so that the plateau present in Fig. 3b is now absent in this representation. In Fig. 4 we can see that all experiments have a similar linear dependence with the hy-

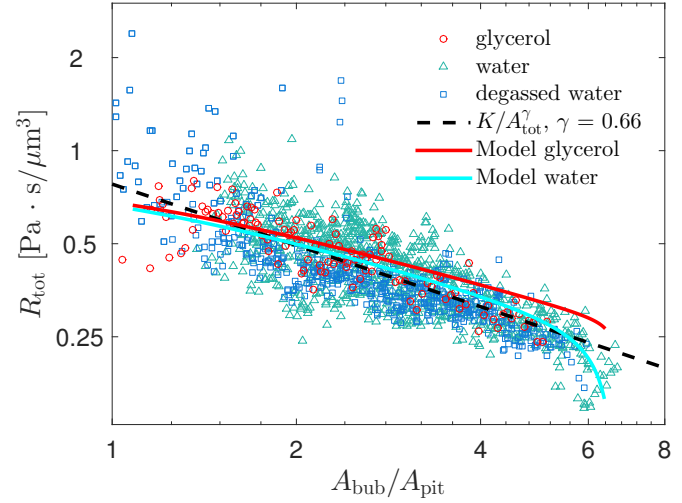


Fig. 5 Resistance to gas flow $R_{\text{tot}} = \Delta p^{\text{air}}/Q_{\text{tot}}$ as a function of the bubble area in the experiments with glycerol, air-saturated water and degassed water (symbols). The solid lines are theoretical results from the model developed in the main text. The dashed line is a power-law fit to the data corresponding to the equation: $R_{\text{tot}} = K/A_{\text{tot}}^\gamma$, with $\gamma = 0.66$ and $K = 1.17 \cdot 10^{13} \text{ Pa} \cdot \text{s}/\text{m}^{3-2\gamma}$. The data points correspond to all measured stages in the growing process for all given hydrostatic pressures (see Fig. 3 a).

drostatic pressure, differing only in their horizontal position in the plot – the experiments with water show growth rates that are displaced to higher pressures, independent of the liquid's gas content. We will show below that such a displacement can be explained by taking into account the liquid vapor pressure.

4 Discussion

The most relevant difference between experiments with water and glycerol is the significantly higher, and temperature dependent vapor pressure of the former in comparison to the latter. Consequently, the gas inside the bubble (as well as the air surrounding the set-up) contains a certain amount of vapor, and the air partial pressure difference can be rewritten as

$$\Delta p^{\text{air}} = p_{\text{bub}}^{\text{air}} - p_0^{\text{air}} = p_{\text{hyd}} + p_{\text{YL}} - (p_{\text{bub}}^{\text{v}} - p_0^{\text{v}}) \quad (2)$$

with $p_{\text{bub}}^{\text{v}}$ and p_0^{v} the vapor pressures in the bubble and surrounding atmosphere, respectively. Thus, the growth curve for water in Fig. 4 should be shifted with respect to that for glycerol by the difference in vapor pressures Δp^{v} . At small Q_{tot} , we read off a pressure difference of circa 4600 Pa, which is indeed in agreement with Δp^{v} : Experiments were performed at 20°C room temperature and 20% humidity, while in the bubble we expect to have 100% humidity as well as an elevated

temperature due to the focused halogen lighting. Assuming a temperature of 33°C inside the bubble, the vapor pressure difference Δp^v takes the value observed in Fig. 4.

These considerations allow for a prediction of the required hydrodynamic pressure for stabilization of a bubble, given the environmental conditions. Note that degassing of the water makes hardly any difference, because the relatively small volume of water in the microchannel is surrounded by gas-permeable PDMS, so that it quickly re-equilibrates (saturates with air). This can be estimated by the time it takes for gas to diffuse through the liquid layer of depth D (and thus establish quasi-static equilibrium) as $\tau_D \sim D^2/D_{\text{air}}^w \approx 5$ s. Therefore we assume that water within the PDMS device gets quickly saturated with air, regardless of its initial state; the detailed time scale depends on the size of the PDMS layer and on the room humidity. These arguments lead us to the conclusion that the rate-limiting step in the growth process is the transport of air from the bubble through the PDMS layer.

The air exchange at the rate Q_{tot} is driven by Δp^{air} , the difference between the air partial pressure inside the bubble $p_{\text{bub}}^{\text{air}}$ and the atmospheric air partial pressure p_0^{air} ; this exchange is slow and should follow a Darcy-like law,²² such that:

$$Q_{\text{tot}} = \Delta p^{\text{air}}/R_{\text{tot}}, \quad (3)$$

where R_{tot} represents the resistance encountered by the air as it is transported through the PDMS and the liquid layer. The value of R_{tot} depends on the geometry of the system and on a non-trivial combination of the permeabilities of PDMS and liquid to air. In the particular case of glycerol, given its negligible vapor pressure,²³ we can safely assume that $p_{\text{bub}} = p_{\text{bub}}^{\text{air}}$ (see Eq. (1)).

Beyond predicting stable bubbles, it is also valuable to describe the time scales of gas exchange for growing and shrinking bubbles, i.e., to quantify the resistance R_{tot} in (3) as a function of the bubble size and/or shape, which is itself time-dependent. The total gas flow rate Q_{tot} is the sum of the flow rate of gas leaving the bubble directly through the PDMS, Q_s , and that of gas transported through the channel liquid (and from there through further PDMS layers surrounding the channel), Q_l . The two contributions are governed by different geometries: the contact surfaces of gas with PDMS consists of the side channel surface and, if the bubble has grown beyond the side channel, the four contact areas with the main channel walls. By contrast, the gas/liquid interface is either flat or semicylindrical – i.e., most of the solid angle of gas exchange is effected through the solid. This fact, as well as the dimensions of the bubble being at least one order of magnitude smaller than the dimensions of the surrounding PDMS walls, and the good agreement of bubble volume change with the radial-symmetry law $V \propto t^{3/2}$ (see log-log plot in the insert of Fig. 3a and supplementary data), suggests describing a bubble surrounded by the liquid layer towards the main channel

and the PDMS substrate on all other sides, as a compact gas pocket that possesses an effective radial extent r_s (the position where the boundary conditions between bubble and PDMS are applied when the gas exchange is modeled as radially symmetric). Focusing on the case where the bubble is semi-cylindrical of radius a , and assuming that the concentration profile of gas in the liquid is quasi-stationary in the cylindrical symmetry of this problem, closed solutions are available for the diffusion equation.²⁴ Combined with a boundary condition given by Henry's law at the gas-liquid interface, it is easy to derive the following formula for this portion of the transport:

$$R_s = \Delta p^{\text{air}}/Q_s = (\Omega_s K_s r_s)^{-1} \quad (4)$$

where the constant $K_s = \kappa/\mu$, with μ the viscosity of air and κ the permeability of PDMS. Values for K_s are directly available in the literature, but vary according to the precise composition and cross-linking of the PDMS. We use the values of de Jong *et al.*¹⁸ for the permeabilities for N₂ and O₂, weighted by their relative fractions, to obtain an effective value of $K_s \approx 350$ barrer = 2.6×10^{-15} m²/(Pa s). The radial scale r_s is determined by the surface area $A_s = \Omega_s r_s^2$ of the bubble-PDMS interface, if this transport affects a solid angle Ω_s .

The transport of gas through the liquid is governed by the flux through the bubble surface. Focusing on the case where the bubble is semi-cylindrical of radius a , and assuming that the concentration profile of gas in the liquid is quasi-stationary in the cylindrical symmetry of this problem (cf.²⁵), it is easy to derive the following formula for this portion of the transport:

$$R_l = \Delta p^{\text{air}}/Q_l = -\ln(a/r_{\text{int}}) (\pi K_l D)^{-1}. \quad (5)$$

Here, r_{int} is the typical distance from the bubble center to the liquid/PDMS interface (so we set $r_{\text{int}} = H$), while the diffusive gas transport is governed by the constant $K_l = v_m D_{\text{air}}^w k_H$, where v_m is the ideal gas molar volume, D_{air}^w was given above and $k_H \approx 7.9 \times 10^{-4}$ mol m⁻³ Pa⁻¹ is the Henry's law constant. For the system air/water, $D_0 \approx 2 \times 10^{-9}$ m²s⁻¹ and $k_H \approx 8.5 \times 10^{-6}$ mol m⁻³ Pa⁻¹. For the system air/glycerol we estimated a value of K_l at least one order of magnitude smaller than that of air/water based on the values found in the literature^{26,27} (see also the calculations in the supplementary material).

Combining (4) and (5) yields a prediction for the dependence of the total transport resistance $R_{\text{tot}} = \Delta p^{\text{air}}/Q_{\text{tot}}$ on the bubble radius a . Assuming that $\Omega_s = 2\pi$ (partitioning the transport into half-spaces of solid and liquid transport), we can rewrite this relation in terms of $A_{\text{tot}} = A_l + A_s$, where

$$A_l = \pi a D \quad (6)$$

and

$$A_s = 2\pi r_s^2 = \pi a^2 + 2aD + 2(D+W)L. \quad (7)$$

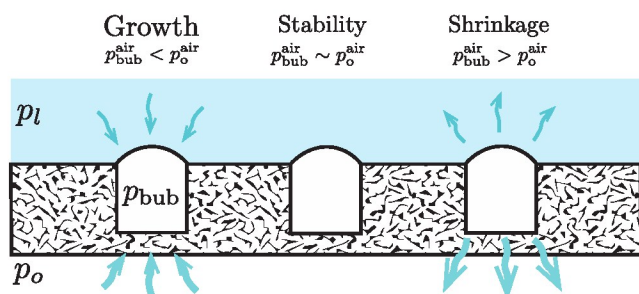


Fig. 6 Illustration on the bubble stabilization mechanism based on the control of hydrostatic pressure of the liquid p_l . The air flow through the solid/liquid media surrounding the bubble is driven by the difference between the air partial pressure inside the bubble $p_{\text{bub}}^{\text{air}}$ and the atmospheric air partial pressure p_o^{air} .

A sketch with the area calculation is included in the supplementary material. Figure 5 shows the experimental results for this relation $R_{\text{tot}}(A_{\text{bub}})$, using the permeability data given above for water, and merely correcting the data for glycerol by the vapor pressure difference. Also shown are the theoretical predictions from Eq. (3) – (7), with $R_{\text{tot}}^{-1} = R_s^{-1} + R_l^{-1}$, as well as the best-fit power law. As resistance is by definition independent of the materials involved, the agreement of values for glycerol and water are a successful test of consistency for both experiment and theory. Theory and experiment agree that this transport relation is somewhat steeper than what would be expected for a purely radial Darcy transport (which would result in $\Delta p^{\text{air}}/Q_{\text{tot}} \propto 1/A_{\text{tot}}^{1/2}$), which is attributable to the transport through the liquid. Without adjustable parameters, the theory developed above captures the magnitude of gas flow with good accuracy, including the strong drop in resistance around $A_{\text{bub}}/A_{\text{pit}} \approx 6$, where (in both experiment and theory) the growing bubble radius becomes comparable to H , so that the vanishing liquid layer offers almost no resistance to gas transfer and the bubble grows faster.

5 Conclusions

In cases where the substrate is totally impermeable to gas transfer (e.g. in silicon devices), the control of the bubble shape can be performed by either controlling the temperature or the amount of gas dissolved in the liquid, which is exchanged with the bubble by diffusion. In our experiments, we demonstrate that bubble growth and shrinkage in permeable materials is dominated by the diffusive transport of gas through its surrounding media, which actually allows for a higher degree of control and more accurate predictions when all transport processes are properly taken into account. By simply controlling the liquid's hydrostatic pressure, one can control the bubble's air partial pressure and its

growth/shrinkage (see Fig. 6). The critical value of the hydrostatic pressure for stability depends only on the Young-Laplace pressure of the bubble and on the vapor pressure of the liquid employed. The latter is a crucial, and unappreciated, element in this situation – changing vapor pressure by moderate changes in temperature can have decisive effects on bubble stability (far surpassing the effect of temperature on gas solubility or other transport parameters). Likewise, relative humidity in the laboratory can be an important factor, so that reproducible experiments using microbubbles in PDMS devices with aqueous solutions should be performed at controlled humidity.

Note that in cases in which a net flow is driven inside the channel, a pressure gradient will develop along the channel and the pressure in the liquid will not be constant. Alternatively, the liquid pressure can then be controlled by connecting the outlet to a pressurized reservoir and adjusting the pressure inside the reservoir. Another option when using volatile liquids is to control the temperature of the system, and therefore to adapt the gas pressure inside the bubble mainly by altering the equilibrium vapor pressure. In the commonly used geometries in microfluidic channel devices, we find that the resistance to gas flow through the system can be accurately modeled if the bubble geometry is properly taken into account. Additionally, the presence of a net flow might increase the relative importance of convective transport of air in comparison to the diffusive transport through the water liquid phase. However, since the key of the bubble stability relies on the transport through the PDMS rather than through the liquid phase, the influence of convective transport terms is minor (see calculations included in the supplementary material).

In summary, in this paper we demonstrate how crucial is the choice of materials and liquids when working with microbubbles in microfluidic applications. We also show that, if the gas transfer problem is well understood, the permeability of commonly-used materials such as PDMS can actually become an advantage when working with multiphase flows in microsystems, membraneless exchangers, transport over bubble mattresses²⁸ or bioreactors.²⁹

Acknowledgements

Abundant discussions and technical help from Kilian Eckstein, Rune Barnkob, and Rocio Bolaños-Jiménez is greatly appreciated. A.V., M.R., A.M. and C.K. acknowledge financial support by the German Research Foundation grant KA 1808/17-1. S.H. acknowledges support by the National Science Foundation under grant number CBET-1236141. The authors are grateful to Cheng Wang for providing the PDMS devices.

References

- 1 G. Liger-Belair, *J. Agric. Food Chem.*, 2005, **53**, 2788–2802.
- 2 A. Prosperetti, *Physics of Fluids*, 2004, **16**, 1852.
- 3 N. Kantarci, F. Borak and K. Ulgen, *Process Biochemistry*, 2005, **40**, 2263–2283.
- 4 Y. S. Shin, K. Cho, S. H. Lim, S. Chung, S.-J. Park, C. Chung, D.-C. Han and J. K. Chang, *J. Micromech. Microeng.*, 2003, **13**, 768–774.
- 5 H.-B. Liu, H.-Q. Gong, N. Ramalingam, Y. Jiang, C.-C. Dai and K. M. Hui, *J. Micromech. Microeng.*, 2007, **17**, 2055–2064.
- 6 O. R. Enríquez, C. Hummelink, G.-W. Bruggert, D. Lohse, A. Prosperetti and C. Sun, *Rev. Sci. Instrum.*, 2013, **84**, 1.
- 7 J. Rodríguez-Rodríguez, A. Casado-Chacón and D. Fuster, *Physical Review Letters*, 2014, **113**, 214501.
- 8 S. Shim, J. Wan, S. Hilgenfeldt, P. D. Panchal and H. A. Stone, *Lab on a Chip*, 2014, **14**, 2428–2436.
- 9 P. Peñas-López, M. A. Parrales and J. Rodríguez-Rodríguez, *Journal of Fluid Mechanics*, 2015, **775**, 53–76.
- 10 P. Marmottant and S. Hilgenfeldt, *Nature*, 2003, **423**, 153–156.
- 11 P. Marmottant and S. Hilgenfeldt, *Proceedings of the National Academy of Sciences of the United States of America*, 2004, **101**, 9523–9527.
- 12 C. Wang, S. V. Jalikop and S. Hilgenfeldt, *Applied Physics Letters*, 2011, **99**, 034101.
- 13 P. Marmottant, J. Raven, H. Gardeniers, J. Bomer and S. Hilgenfeldt, *Journal of Fluid Mechanics*, 2006, **568**, 109–118.
- 14 P. S. Epstein and M. S. Plesset, *The Journal of Chemical Physics*, 1950, **18**, 1505–1509.
- 15 Y. Xia and G. M. Whitesides, *Annual review of materials science*, 1998, **28**, 153–184.
- 16 T. Merkel, V. Bondar, K. Nagai, B. Freeman and I. Pinnau, *Journal of Polymer Science Part B: Polymer Physics*, 2000, **38**, 415–434.
- 17 G. C. Randall and P. S. Doyle, *Proceedings of the National Academy of Sciences*, 2005, **102**, 10813–10818.
- 18 J. De Jong, R. Lammertink and M. Wessling, *Lab Chip*, 2006, **6**, 1125–1139.
- 19 C. Wang, S. V. Jalikop and S. Hilgenfeldt, *Biomicrofluidics*, 2012, **6**, 012801.
- 20 P.-G. De Gennes, F. Brochard-Wyart, D. Quéré, *Capillarity and wetting phenomena: drops, bubbles, pearls, waves*, Springer, 2004.
- 21 S. M. Thomas and Y. Chan, *Computer Vision, Graphics, and Image Processing*, 1989, **45**, 362–370.
- 22 H. Darcy, *Les fontaines publiques de la ville de Dijon*, Victor Dalmont, 1856, **7**, 710–719.
- 23 D. R. Lide, *CRC handbook of chemistry and physics*, CRC press, 2004.
- 24 B. C. Craft, M. F. Hawkins and R. E. Terry, *Applied petroleum reservoir engineering*, Prentice-Hall Englewood Cliffs, NJ, 1959, vol. 199.
- 25 H. S. Carslaw and J. C. Jaeger, *Conduction of heat in solids*, Oxford: Clarendon Press, 1959, 2nd ed., 1959, vol. 1.
- 26 E. Rischbieter, A. Schumpe and V. Wunder, *Journal of Chemical & Engineering Data*, 1996, **41**, 809–812.
- 27 W. Thomas and M. Adams, *Transactions of the Faraday Society*, 1965, **61**, 668–673.
- 28 E. Karatay and R. G. H. Lammertink, *Lab Chip* 2012, **12**, 2922–2929.
- 29 E. Figallo, et al., *Lab Chip* 2007, **7**, 710–719.